THE JOURNAL OF PHYSICAL CHEMISTRY B

Article

pubs.acs.org/JPCB

Pressure Effects on Emim[$FeCl_4$], a Magnetic Ionic Liquid with Three-Dimensional Magnetic Ordering

Abel García-Saiz,[†] Imanol de Pedro,*[,†] Jesús A. Blanco,[‡] Jesús González,[§] and Jesús Rodríguez Fernández[†]

[†]CITIMAC & MAGMA, Unidad Asociada-CSIC, Facultad de Ciencias, Universidad de Cantabria, 39005 Santander, Spain

[‡]Departamento de Física, Universidad de Oviedo, 33007 Oviedo, Spain

[§]MALTA Consolider Team, CITIMAC, Facultad de Ciencias, Universidad de Cantabria, 39005 Santander, Spain

Supporting Information

ABSTRACT: We report a combined study using magnetization and Raman spectroscopy on the magnetic ionic liquid 1-ethyl-3-methylimidazolium tetrachloroferrate, Emim[$FeCl_4$]. This material shows a long-range antiferromagnetic ordering below the Néel temperature $T_N \approx 3.8$ K. The effects of pressure on the magnetic properties have been studied using a miniature piston−cylinder CuBe pressure cell. This three-dimensional ordering is strongly influenced when hydrostatic pressure is applied. It is observed that low applied pressure is enough to modify the magnetic interactions, inducing a transition from antiferromagnetic to ferrimagnetic ordering. Raman spectroscopy measurements reveal important information about the existence of isolated $[FeCl_4]^-$ anions and the absence of dimeric $[Fe_2Cl_7]^-$ units in the liquid and solid states. These features seem to suggest that the superexchange pathways responsible for the appearance of magnetic ordering are mediated through Fe-Cl−Cl-Fe. Furthermore, the liquid−solid phase transition exhibits a magnetic hysteresis near room temperature, which can be tuned by weak pressures.

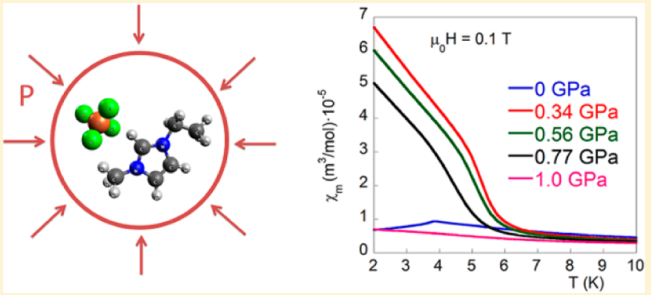

INTRODUCTION

Room-temperature ionic liquids (RTILs)[1] are molten salts with their melting point near room temperature. They are formed of organic cations, generally with imidazolium, pyrrolidium, pyridinium, tetraalkylammonium, or tetraalkylphosphonium ions, and anions (e.g., Cl^-, Br^-, I^-, $FeCl_4^-$, PF_6^-, $AlCl_4^-$, BF_4^-, NO_3, ...).[2] These compounds have been the focus of study over the last few decades because of their interesting physicochemical properties,[3] such as negligible vapor pressure, wide liquid range, good thermal stability, considerable electric conductivity, chemical stability, etc. Besides, the broad range of ion compositions opens up an unlimited number of possibilities for new materials and applications, such as batteries,[4] fuel cells,[5] optical sensors,[6] photovoltaic cells,[7] catalysis,[8] etc. Room-temperature magnetic ionic liquids (RTMILs) are the latest development of RTILs, promising new materials that will allow further features to be added to the typical properties of ILs, such as magnetic, photophysical/optical,[9] or electrochromic[10] behavior, all of which are due to the incorporated metal. They were discovered in 2005 by Hayashi et al.[11] in studies carried out on 1-butyl-3-methylimidazolium tetrachloroferrate Bmim-[$FeCl_4$], which has a paramagnetic behavior with an effective moment of 5.8 μ_B. Typically, MILs are composed of metal-containing anions, such as iron, cobalt,[12] manganese,[13] copper,[14] etc. Nowadays, the development of these MILs has led to different rare-earth[15] (neodymium,[16] gadolinium, dysprosium[17]), chiral amionacids (MCILs),[18] or bimagnetic ions[19] being combined. Therefore, the synthesis, study, and application of these new materials are growing exponentially.[20]

As regards to the technological applications of MILs, due to their high magnetic response to external magnetic fields, they can be used for the transport and separation of materials,[21] as an absorbent for benzene emissions,[22] catalysis,[23] sulphide (SO_x) extraction in gasoline,[24] a greenhouse effect gas (CO_2 and SO_2) absorbent,[25] new magnetic applied materials,[26] or biotechnology.[27] As such, it is necessary to understand the magnetic behavior of these new materials in order to improve or develop these potential applications.

Up to now, most of the magnetic ionic liquids have evidenced a paramagnetic behavior with small deviations from the Curie law at low temperatures, indicating a lack of long-range interaction between metal ions. In addition, the reported structures found in the literature show that no magnetic coupling pathways are observed since distances between metal ions are so large as to allow significant long-range magnetic interactions. This is not the case of 1-ethyl-3-methyl-imidazolium tetrachloroferrate, Emim[$FeCl_4$], which shows a three-dimensional ordering near 4 K.[28,29] A recent study by Bäcker et al.[30] has shown that, below 280 K, this MIL crystallizes in a monoclinic space group $P21/c$ (a = 9.424(3) Å, b = 14.662(4) Å, c = 12.449(9) Å, β = 129.89(2)°, V =

Received: November 20, 2012
Revised: February 21, 2013

   dx.doi.org/10.1021/jp3114623 | J. Phys. Chem. B XXXX, XXX, XXX−XXX

1319.2(4) Å^3). The crystal structure can be described as formed by layers of cations and anions, alternating along the *b* direction showing Fe−Fe direct distances larger than 6 Å (see the Supporting Information, Figure S1). The anion groups $[FeCl_4]^-$, with four iron ions in the unit cell, are slightly distorted in the *a*,*c* plane, the orientation changing from layer to layer. The $Emim^+$ cations are stacked nearly identically one above the other, and lie antiparallel to each other along the *c* direction. Infrared and Raman spectroscopies as a function of pressure have been widely used on RTILs for structural investigations, showing significant changes of their molecular conformation or phase transitions.[31] Since studies on the effects of pressure in RTMILs are scarce, we have performed a thorough study aiming to investigate how the structural and magnetic properties of RTMILs can be tuned by the pressure effect. In this paper, we report the magnetic behavior under hydrostatic pressure of $Emim[FeCl_4]$, showing a pressure-induced transition from antiferromagnetic to ferrimagnetic three-dimensional ordering. In addition, Raman measurements of $Emim[FeCl_4]$ under pressures up to about 1 GPa were collected using a high-pressure membrane diamond anvil (MDAC) apparatus. The MDAC was mounted under a microscope for the visual observation of the liquid−solid phase transition.

EXPERIMENTAL SECTION

$Emim[FeCl_4]$ is a magnetic ionic liquid provided by TCI Europe (Belgium) with a purity above 99% with a nonmagnetic impurity of 1-ethyl-3-methylimidazolium chloride. For the magnetic study, 15.82 mg of $Emim[FeCl_4]$ was contained in a sealed Teflon capsule. Magnetic measurements were performed in a Quantum Design MPMS (SQUID) magnetometer at temperatures in the range of 2−300 K and magnetic fields of up to 5 T. Applied pressure was carried out using a piston−cylinder-type MCell pressure cell enabling pressures up to 1 GPa to be obtained. The applied pressure was estimated from the superconducting transition temperature of a tiny Sn sample placed inside the cell, with an estimated error of 0.02 GPa.[32]

The room-temperature nonpolarized Raman spectra were obtained in the backscattering geometry with a Horiba T64000 triple spectrometer with a confocal microscope in the single mode equipped with an edge filter that had a resolution of 1 cm^{-1}, a 1800 grooves/mm grating and a 100 μm slit and was equipped with a liquid N_2-cooled CCD detector (Jobin-Yvon Symphony). A 514.5 nm line of a Coherent Innova Spectrum 70C Ar^+−Kr^+ laser was focused down with a 20× objective. The power on the sample was kept below 5 mW to avoid laser-heating effects on the probed material and the concomitant softening of the observed Raman peaks. For the high-pressure experiments, we used two types of pressure cells. On one hand, a membrane diamond anvil cell (MDAC) with two diamond anvils of 500 μm of culet size and a very low fluorescence (Type IIa) was used to visualize the liquid to solid phase transition induced by pressure. On the other hand, a Merril-Basset pressure cell equipped with two SiC (moissonite) anvils, with a 600 μm culet, was employed to avoid the interference from the dominant diamond Raman band (T_{2g}). The liquid sample and the ruby chips were placed in the 200 μm diameter hole of the stainless-steel gasket preindented to a thickness of 40 μm, together with spectroscopic paraffin oil as a pressure-transmitting medium. Pressure was determined by the ruby luminescence method using a linear variation coefficient, with an estimated error of 0.03 GPa.[33]

RESULTS AND DISCUSSION

Magnetic Measurements. The field-cooled (FC) magnetic susceptibility (χ_m) measured under 0.1 T at different pressures from 0 to 1.0 GPa is shown in Figure 1. It can be seen

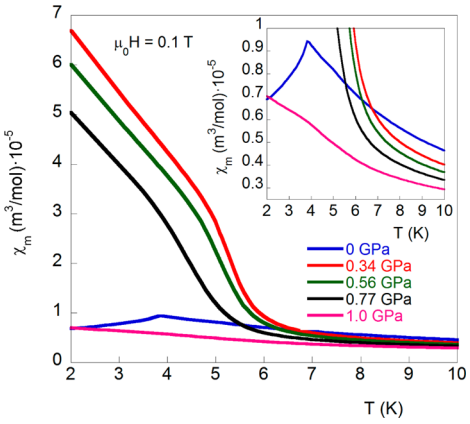

Figure 1. Low-temperature dependence of the FC magnetic susceptibility measured under an applied magnetic field of 0.1 T at different pressures from 0 to 1.0 GPa. The inset shows an enlargement of the low magnetic susceptibility data.

that, without pressure, the magnetic susceptibility displays a small peak at 3.8 K (see inset of Figure 1), which corresponds to the onset of the three-dimensional ordering.

The shape of the susceptibility at low temperatures changes drastically (see Figure 1) when the applied pressure increases from 0 to 0.34 GPa. Below 6 K, a strong increase in χ_m with a new inflection point close to 5 K appears. It then continues to increase as temperatures drop down to 2 K, indicating a possible ferrimagnetic ordering with a Curie temperature (T_C) of 5.3 K. This magnetic behavior is maintained for the pressures of 0.56 and 0.77 GPa. In this intermediate pressure range, the only effect of increasing the pressure is a small decrease in both the absolute value of χ_m below 6 K and T_C (see Table 1). Finally, for the highest studied pressure (P = 1.0 GPa), the shape of the experimental curve does not change significantly, although the values of χ_m decrease drastically, approaching those obtained without pressure (see inset of Figure 1).

The pressure dependence of the reciprocal susceptibility $1/\chi_m$ versus temperature is shown in Figure 2 (for reasons of clarity, only up to 16 K are plotted). Without pressure, above 10 K, the thermal evolution of χ_m follows the Curie−Weiss law with paramagnetic Curie temperature θ_P = −1.4 K and an effective paramagnetic moment of μ_{eff} = 5.78 μ_B/Fe, which is consistent with a high-spin state of S = 5/2 in Fe^{3+}. The paramagnetic Curie temperature is negative, indicating that the major magnetic interactions in the compound are antiferromagnetic. These results are in good agreement with the previous studies,[28,29] where the θ_P and μ_{eff} were −2.5 K and 5.66 μ_B/Fe, respectively. At the different pressure studies, the paramagnetic susceptibility also follows the Curie−Weiss law at temperatures higher than 12 K, but on approaching T_C, the susceptibility deviates from the Curie−Weiss law like a ferrimagnet; that is, the curve of the reciprocal magnetic susceptibility versus temperature just above the Curie temperature is a hyperbola. Therefore, the inverse molar magnetic susceptibility was fitted to the Néel expression [eq 1] for ferrimagnetic materials,[34] in order to analyze the effect of pressure on the magnetic data. These main magnetic

dx.doi.org/10.1021/jp3114623 | J. Phys. Chem. B XXXX, XXX, XXX−XXX

Table 1. Main Magnetic Data of Emim[$FeCl_4$] at Different Pressures, where P is Pressure, T_N and T_C are the Néel and Curie Temperatures, θ_P and C are the Paramagnetic Curie Temperature and the Curie Constant, respectively, μ_{eff} is the Effective Paramagnetic Moment, γ and Θ Are Fitting Parameters, and M is the Magnetization

P (GPa)	T_N or T_C (K)	θ_P (K)	μ_{eff} (μ_B/Fe)	$C\cdot10^{-5}$ (m^3 K/mol)	γ 10^5 (mol K/m^3)	Θ (K)	M (μ_B/Fe) 2 K, 5 T
0	3.8(1)	−1.4(1)	5.78(1)	5.25(1)			4.43(1)
0.34	5.3(1)	−4.1(1)	5.77(1)	5.23(1)	1.11(1)	4.67(1)	3.43(1)
0.56	5.1(1)	−6.2(1)	5.85(1)	5.38(1)	1.71(1)	4.29(1)	3.09(1)
0.77	4.5(1)	−6.7(1)	5.73(1)	5.15(1)	1.53(1)	4.10(1)	2.71(1)
1.0	4.4(1)	−7.9(1)	5.64(1)	4.99(1)	1.35(1)	2.85(1)	2.50(1)

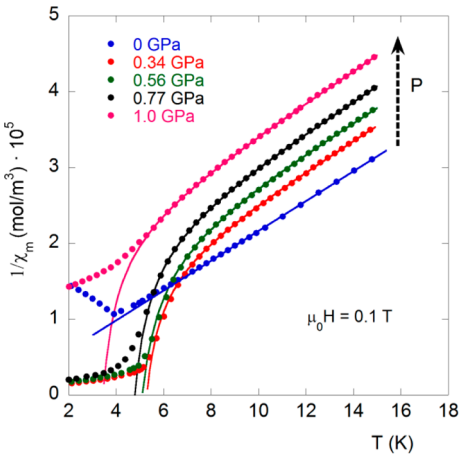

Figure 2. Temperature dependence of the $1/\chi_m$ under different pressures. Continuous lines represent the fitting to the modified Curie−Weiss law according to eq 1.

parameters are included in Table 1 for comparison with those obtained without pressure.

$$\chi^{-1} = \frac{(T - \theta_P)}{C} - \frac{\gamma}{T - \Theta} \quad (1)$$

In the expression, θ_P and C are the paramagnetic Curie temperature and the Curie constant, respectively. Θ and γ are fitting parameters that depend on the molecular field coefficients associated with the coupling of the magnetic moments of the different magnetic sublattices in the ferrimagnetic material. The best fits obtained (see continuous line in Figure 2) show a θ_P value of −4.1 K for 0.34 GPa, which decreases to −7.9 K as the pressure increases up to 1.0 GPa. The value of μ_{eff} obtained from the Curie constant ranges from 5.64 to 5.85 μ_B/Fe ion (see Table 1), being slightly smaller than the theoretical effective paramagnetic moment for a highly isotropic Fe^{3+} ion (L = 0, S = 5/2, and μ_{eff} = 5.92 μ_B/Fe). Because θ_P represents the sum of all the superexchange interactions, its pressure dependence reveals that antiferromagnetic interactions rise as the applied pressure increases. In addition, the value of θ_P/T_C enhances with the applied pressure (from 0.8 to 1.8 for P = 0.34 and 1.0 GPa, respectively), revealing the presence of higher magnetic frustration in the magnetic structure.

For a deeper understanding of the effect of pressure, the magnetic susceptibility as a function of temperature at different applied magnetic fields and pressures has been studied (Figure 3). Without pressure (not shown), the peak observed at approximately 4 K shifts to lower temperatures when the field increases and the susceptibility shows no irreversibility for any field, as expected for an antiferromagnetic behavior.[29] For a pressure of 0.34 GPa, the ZFC−FC curves at 0.01 T show a small irreversibility below 6 K that could be attributed to the existence of magnetic domains (Figure 3a). This magnetic irreversibility decreases as the applied field increases and disappears for magnetic fields higher than 0.05 T. For the pressures of 0.56 and 0.77 GPa, the magnetic behavior is similar (see the Supporting Information, Figure S2), presenting irreversibility for low applied fields. What should be mentioned is the change of the magnetic curves for the pressure of 1.0 GPa (see Figure 3b). For an applied magnetic field of 0.01 T, the ZFC−FC curve shows a complex magnetic behavior with the presence of two different characteristic temperatures. First, the χ_m increases as the temperature decreases, showing an inflection point near 4 K. A sharp decrease then begins at 2.6

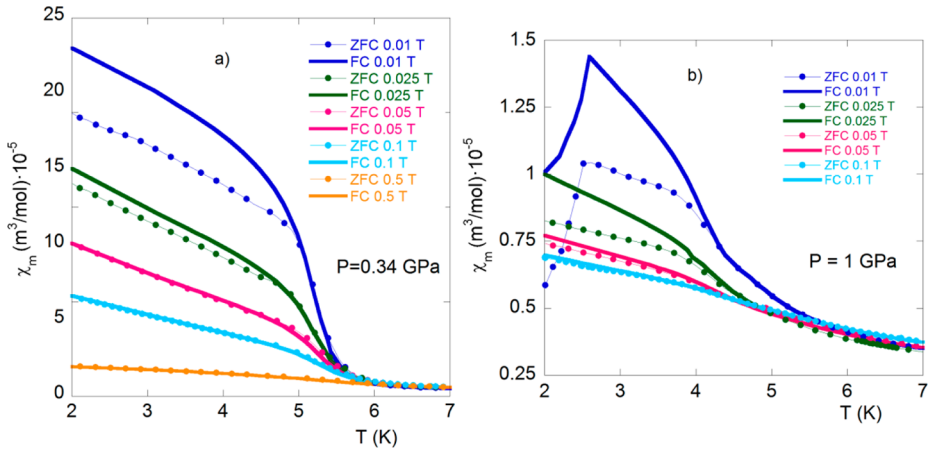

Figure 3. Low-temperature ZFC−FC magnetic susceptibility for different magnetic fields from 0.01 to 0.5 T under pressures of (a) 0.34 GPa and (b) 1.0 GPa.

dx.doi.org/10.1021/jp3114623 | J. Phys. Chem. B XXXX, XXX, XXX−XXX

K and continues down to the lower measured temperature of 2 K. Furthermore, irreversibility appears below 4.2 K, which corresponds with the Curie temperature. As can be seen, the magnetic field bears influence on both magnetic features (irreversibility and sharp decrease). The irreversibility decreases with increasing applied magnetic fields, and disappears for fields higher than 0.05 T, while the sharp decreasing of the magnetic susceptibility at low temperature is not visible for fields larger than 0.025 T. A similar shape in the susceptibility curves and also a comparable field dependence has been reported in a ferrimagnetic insulating compound, $ND_4Fe(DPO_4)_2$.[35] The authors have reported that this magnetic behavior is due to a complex magnetic structure with two types of magnetic sublattices of the Fe^{3+} ion. The neutron powder diffraction experiments showed that temperature induced slight geometrical differences in the parameters of the magnetic structure pathways (angles and interatomic distances). That produced a magnetic phase transition from a ferrimagnetic to an antiphase magnetic structure[35] for temperatures below the sharp drop.

The field dependence of the magnetization at 2 K for different pressures is depicted in Figure 4. Without pressure, the magnetization shows a linear dependence from 0 to 3 T, and then it tends to saturate. At 5 T, the value of the magnetic moment is near the theoretical saturation moment expected for Fe^{3+} ions with a magnetic spin $S = 5/2$ (5 μ_B/Fe). Furthermore, the magnetization curve without pressure shows no hysteresis, suggesting the absence of any ferromagnetic component (see inset of Figure 4). This behavior is clearly different for that observed for the applied pressures of 0.34, 0.56, and 0.77 GPa, in which a metamagnetic transition appears around 3 T. At low fields, a fast increase in the magnetization up to 0.5 T is observed, corresponding to the alignment of the magnetic domains. It then shows an almost constant value of $M = 1.5\ \mu_B$/Fe up to 2, 2.5, and 3 T for 0.34, 0.56, and 0.77 GPa, respectively. This value is slightly lower than one-third of the theoretical saturation moment expected for an $Fe^{3+}(3d^5)$ free magnetic moment ($\mu = 2S$, $M = 5\ \mu_B$). It is worth noting that this one-third magnetization plateau may be attributed to the existence of two "up" and one "down" magnetic moment, following the arrangement ↑↓↑, in accordance with a ferrimagnetic ordering. After the metamagnetic process, the magnetization starts increasing again, since the magnetic field is strong enough to flip the moments, reaching a magnetization value of 3.43, 3.09, and 2.71 μ_B/Fe at 5 T for 0.34, 0.56, and 0.77 GPa, respectively. It should be mentioned that these values are still far from the theoretical saturation value, indicating a strong magnetic anisotropy, which rises as the applied pressure increases. For the highest pressure studied (P = 1.0 GPa), the shape of the magnetization curve changes significantly, showing a small curvature below 1 T and then an almost linear behavior up to 5 T. At this field, the magnetization is 2.50 μ_B/Fe, slightly smaller than those for previous pressures. Finally, in all the $M(H)$ curves under applied pressure, a magnetic irreversibility (hysteresis loop) is observed below 0.1 T, with a coercitive field ($\mu_0 H_C$) and remanent magnetization (M_r) values lower than 0.09 T and 0.15 μ_B/Fe (see inset of Figure 4). In particular, it is observed that the coercitive field increases with pressure due to the enhancement of the anisotropy, this increase being larger for the highest pressure.

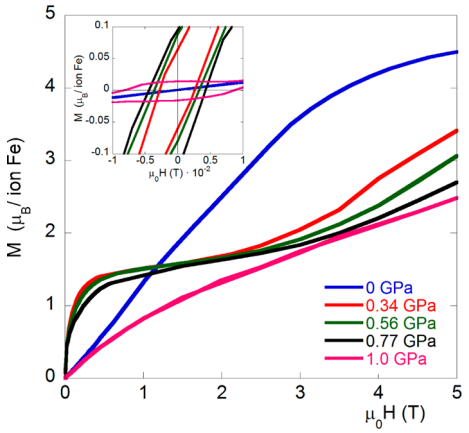

Figure 4. Magnetization vs applied magnetic field at 2 K for different pressures from 0 to 1.0 GPa. The inset shows an enlargement of the low magnetic field region to better observe the increase of the coercitive field with pressure (see text).

It is known that small magnetic fields (<1 T) can control the orientation of several room-temperature ionic liquids during the solidification process.[26,29] The existence of magnetic hysteresis in non-ordered magnetic systems is possible only for materials that are anisotropically packaged. For those systems under these conditions, the physicochemical state should be modified by the application of pressure, creating subsequent effects on the bonding properties of the system. We, therefore, analyzed the effects of pressure on the liquid−solid transition. The temperature dependence of ZFC−FC magnetic susceptibility around room temperature at different applied pressures is shown in Figure 5. When $Emim[FeCl_4]$ is cooled without pressure (see inset of Figure 5), χ_m shows a small jump at 285 K, associated with the liquid−solid transition. After that, when the liquid is warmed with the same magnetic applied field, the susceptibility displays an inflection point at 291 K, related with the melting point.[26,29] Thus, a magnetic hysteresis appears between 285 and 291 K. The same experiment realized at 0.34 GPa showed no hysteresis in the temperature range studied, so we proceeded to do a low-pressure study (below 0.15 GPa). The temperature dependence of ZFC−FC magnetic susceptibility at 0.07 GPa displays a shift in both liquid−solid transition and melting point to 293 and 301 K, respectively. Furthermore, the jump in the susceptibility is lower than that without pressure (0.015×10^{-7} and 0.012×10^{-7} m^3/mol at 0

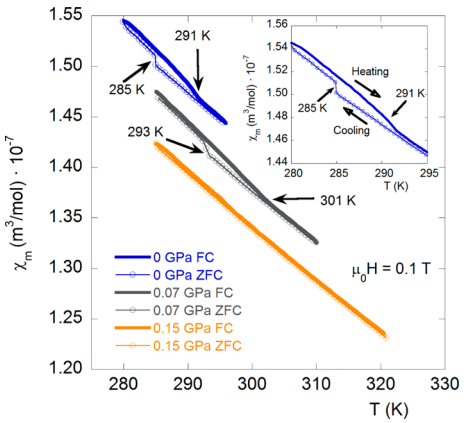

Figure 5. ZFC−FC magnetic susceptibility at temperatures near the melting point measured for 0.1 T under different pressures from 0 to 0.15 GPa. The curves have been shifted 0.03×10^{-7} m^3/mol for clarity.

dx.doi.org/10.1021/jp3114623 | J. Phys. Chem. B XXXX, XXX, XXX−XXX

Table 2. Vibrational Assignment (cm^{-1}) of Emim[$FeCl_4$] at Room Temperature for the Pressures 0, 0.35, and 1.05 GPa[a]

experimental center/cm^{-1}			
0 GPa	0.35 GPa	1.05 GPa	assignation[38]
109	112	117	[$FeCl_4^-$] Fe−Cl sym bend
140	139	142	[$FeCl_4^-$] Fe−Cl asym bend
332	335	337	[$FeCl_4^-$] Fe−Cl sym stretch
377	375	379	[$FeCl_4^-$] Fe−Cl asym stretch
	382	389	[Ethyl] CH_2−N bend, gauche conformer[39,40]
393	398	402	[Ethyl] CH_2−N bend, gauche conformer
	447	450	[Ethyl] CH_2−N bend, trans conformer
595	600	611	[Ring] ip sym bend, [Ethyl] CH_2−N stretch, [Ring CH_3] CH_3−N stretch
645	640	630	[Ring] op asym bend, [Ethyl] CH_2−N stretch, [Ring CH_3] CH_3−N stretch
666	669	701	[Ring] ip asym bend, [Ethyl] CH_2−N stretch, [Ring CH_3] CH_3−N stretch
852	865	862	[Ring] HC═CH asym bend
959	966	969	[Ring] ip sym bend, [Ethyl] C−C stretch
1022	1025	1027	[Ring] ip sym stretch
1032	1033		[Ring] ip sym stretch, [Ethyl] CH_2−N stretch, [Ring CH_3] CH_3−N stretch
1087	1086	1089	[Ring] ip sym stretch, [Ethyl] CH_2−N stretch, [Ring CH_3] CH_3−N stretch
1107	1016	1014	[Ring] ip asym stretch, [Ethyl] C−C stretch, [Ring CH_3] CH_3−N twist
1122	1122	1122	[Ring] ip asym stretch, [Ethyl] C−C stretch, [Ethyl] CH_2−N stretch, [Ring CH_3] CH_3−N stretch
1166	1166	1164	[Ring CH_3] H−C−H bend
1381	1387	1389	[Ring] ip asym stretch, [Ethyl] C−C stretch, [Ethyl] CH_2−N stretch, [Terminal CH_3] CH_3−N stretch
1418	1419	1415	[Ring] ip asym stretch, [Ethyl] C−C stretch, [Ethyl] CH_2−N stretch, [Ring CH_3] CH_3−N stretch
1454	1452	1454	[Ring] ip asym stretch, [Ethyl] C−C stretch, [Ethyl] CH_2−N stretch, [Ring CH_3] C−N stretch
	1468	1470	[Ring] ip asym stretch, [Ethyl] C−C stretch, [Ethyl] CH_2−N stretch, [Ring CH_3] C−N stretch
1587			[Ring] ip asym stretch, [Ethyl] CH_2−N stretch, [Ring CH_3] CH_3−N stretch
2827	2823	2821	[Terminal CH_3] H−C−H sym stretch
2880	2888	2889	[Ring CH_3] H−C−H sym stretch
2919	2922	2922	[Ethyl CH_2] H−C−H sym stretch
2942	2946	2949	[Ethyl] H−C−H asym stretch
2960	2963	2967	[Ethyl] H−C−H asym stretch
2990	2987	2984	[Ethyl] H−C−H asym stretch
		2998	[Ethyl] H−C−H asym stretch
3116	3105	3104	[Ring CH_3] H−C−H asym stretch
	3130	3135	[Ring N−C(H)−N] C−H stretch
	3152	3156	[Ring] HC═CH sym stretch, [Ring] ip sym stretch
3164	3173	3176	[Ring] HC═CH sym stretch, [Ring] ip sym stretch

[a]Note that ip and op are in-plane and out-of-plane vibrations.

and 0.07 GPa, respectively), and it completely disappears up to 320 K for a pressure of 0.15 GPa (see Figure 5). Finally, what should be mentioned is that the initial magnetic behavior is recovered when the pressure is released. Indeed, the results obtained show that the hysteresis can be tuned by small pressures in a reversible process by changing the temperature (isobaric process). When the pressure rises above a critical value (0.15 GPa), the hysteresis disappears. To separate the thermal and volume effects, high-pressure experiments at constant temperature (isothermal process), which will be discussed in the next section, are needed.

Raman Spectroscopy under High Pressure. The study of the mechanisms governing the magnetic interactions between neighboring magnetic units represents a major research goal in magnetic anionic liquids. To understand the magnetic interactions of Emim[$FeCl_4$], the first step is to determine all the possible superexchange magnetic pathways that can transmit the magnetic interaction between two iron ions. The formation of these magnetic units has been evidenced by Raman spectroscopy.[36] Indeed, the conformational analysis of the $Emim^+$ cation and [$FeCl_4$]$^-$ anion under high pressure has been done to obtain structural information on the high-pressure phase of the Emim[$FeCl_4$]. The Raman spectrum of Emim[$FeCl_4$] without pressure at room temperature in the region from 100 to 3500 cm^{-1} is shown in the Supporting Information (see Figure S3). The observed frequencies and their assignments are summarized in Table 2. Of particular interest are the Raman bands observed at 109, 140, 332, and 377 cm^{-1}. These may be compared with the vibrational spectra of free [$FeCl_4$]$^-$ ion, which belong to the symmetry point group T_d, which has four Raman-active vibration modes. Two of them are due to the bending mode, one asymmetric (ν_{as} = 140 cm^{-1}) and the other symmetric (ν_s = 109 cm^{-1}), while the other two are related to the stretching mode (ν_{as} = 377 cm^{-1} and ν_s = 332 cm^{-1}) of the Fe−Cl bond. These observed bands correspond very well with literature values of other MIL with tetrahalogenoferrate(III) anions,[37] indicating that [$FeCl_4$]$^-$ is the predominant iron-containing species in the ionic liquid.

The Raman bands observed between 400 and 3500 cm^{-1} are assigned to the $Emim^+$ cation, and it may be compared with the theoretical and experimental vibrational frequencies reported for other imidazolium-based RTILs, Emim[BF_4].[38] Considering the conformational equilibrium of the $Emim^+$ cation across the CH_2−N bending mode of the ethyl chain [(trans−gauche) (planar−nonplanar)], Umebayashi et al.[39] and Ozawa et al.[40] assigned the Raman bands located at 387, 430, and 448 cm^{-1} to

dx.doi.org/10.1021/jp3114623 | J. Phys. Chem. B XXXX, XXX, XXX−XXX

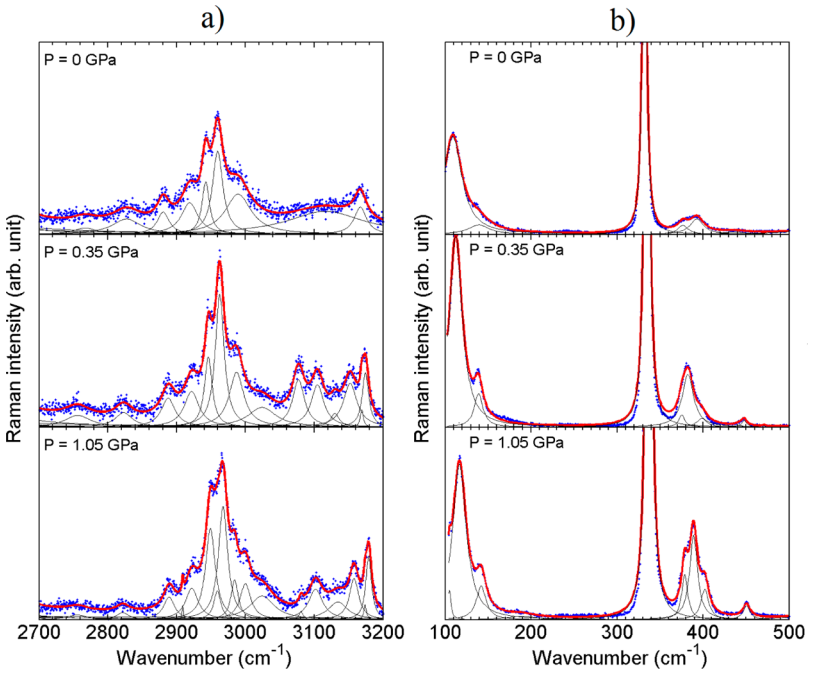

Figure 6. Raman spectrum for the pressures 0, 0.35, and 1.05 GPa in the (a) $FeCl_4$ region and (b) C−H stretch region.

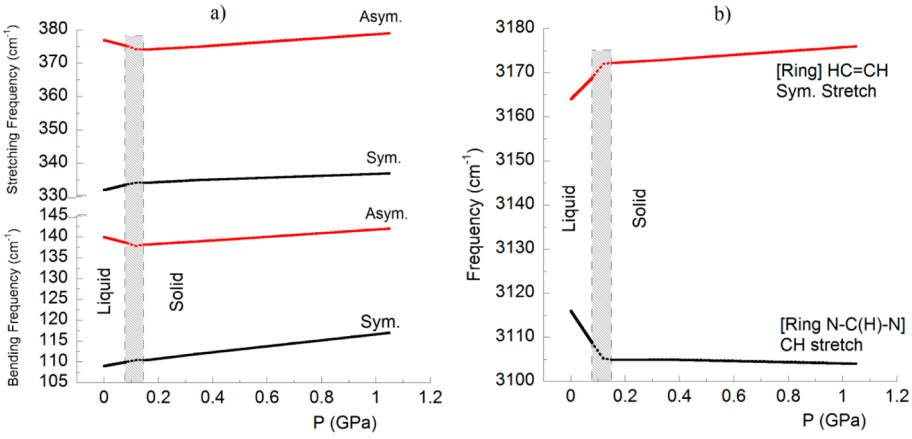

Figure 7. Variation of frequency with pressure for (a) stretching and bending modes for $FeCl_4^-$ ion and (b) the symmetric stretching modes of [ring] HC═CH and [ring N−C(H)−N] C−H. The gray region marks a boundary where phase transition occurs.

the gauche, gauche, and trans conformers, respectively. Thus, the mode located at 393 cm^{-1} for Emim[$FeCl_4$] is attributed to the gauche nonplanar geometry. In addition, we can rule out the presence of $[Fe_2Cl_7]^-$ dimers as no signal is found around 420 cm^{-1}, where the vibrational frequency of the dimer typically appears.[36] The remaining bands observed in the 1000−1600 cm^{-1} region were assigned to the ring in-plane symmetric stretch for trans−gauche conformers (see Table 2).

At higher frequencies, between 2826 and 2960 cm^{-1}, the Raman spectrum of Emim[$FeCl_4$] contains at least four intense bands. The theoretical (B3LYP) calculated vibrations assigned to these peaks include terminal CH_3 (symmetric H−C−H stretch), the ring CH_3 (symmetric H−C−H stretch), the ethyl CH_2 (symmetric H−C−H stretch), and ethyl (asymmetric H−C−H stretch), respectively.[38] In addition, there are at least three (overlapping) weak Raman bands at 3116, 3124, and 3164 cm^{-1}. The theoretical gas-phase vibrations include a ring CH_3 (H−C−H asymmetric stretch), a ring N−C(H)−N (C−H stretch), and a mixture of a ring HC═CH symmetric stretch and a ring in-plane symmetric stretch, respectively.[38]

Figure 6 displays the evolution of the Raman frequencies under pressure up to 1.05 GPa in the spectral range of (a) high and (b) low frequencies, respectively. As the pressure increased, in general, all the Raman bands shifted progressively toward high frequencies, accompanied by peak broadening. Furthermore, we can see conformational changes in the $Emim^+$ cation. On the one hand, the increasing of pressure enhances both the hydrogen bonding, showing a splitting, and the C−H stretching modes of the imidazolium ring.[41] These vibrational bands are located between 3100 and 3200 cm^{-1} (see Table 2 and Figure 6a). On the other hand, a change in the conformational equilibrium of the CH_2−N bending mode of the ethyl chain is detected. The vibrational spectra at 0.35 GPa exhibit new vibrational modes located at 382, 398, and 447 cm^{-1} (see Table 2 and Figure 6b), which correspond to the gauche, nonplanar, and to the trans- conformer planar, respectively. Finally, the compression does not induce changes in vibrational modes of

dx.doi.org/10.1021/jp3114623 | J. Phys. Chem. B XXXX, XXX, XXX−XXX

[$FeCl_4$]. The Raman spectra of the Fe−Cl bond show the same features up to 1.05 GPa, indicating that the tetrahedral structure of the anion is relatively similar in the entire pressure range investigated.

Figure 7 shows some examples of the variation of frequency with pressure for (a) stretching and bending modes for the $FeCl_4^-$ ion and (b) the symmetric stretching modes of [ring] HC═CH and [ring N−C(H)−N] CH. In some cases, there is a softening of the frequencies with pressure and, after the phase transition (defined as gray region), a change in the behavior of the vibration modes, their becoming hardened as the pressure increases (asymmetric bending and stretching $FeCl_4$ and [ring N−C(H)−N] C−H). In other cases, the frequency increases with pressure, showing a slope change after the phase transition, the pressure coefficient being higher before it. Indeed, spectral changes due to the imidazolium ring are larger than those of the $[FeCl_4]^-$ ion, indicating that the environment around the imidazolium ring is more perturbed than that around the $FeCl_4^-$ ion under applied pressure. The liquid structure is modified to favor the components of smaller volume under the application of high pressure. The reported structures of Emim[$FeCl_4$][30] show isolated, discrete tetrahedral anions and no metal-bridging halides, and feature distances larger than 6 Å between next-nearest neighboring metal centers. The formation of dimeric $[Fe_2Cl_7]^-$ units has not been evidenced from Raman spectroscopy under high pressure. The formation of chlorine bridges would allow, in principle, the antiferromagnetic coupling of two Fe^{3+} ions. Therefore, the Fe-Cl−Cl-Fe magnetic interaction, including two diamagnetic intermediaries,[42] should be of the superexchange-pathways mechanism type in Emim[$FeCl_4$].

The microscopic observation of crystalline ionic liquid in the pressure chamber has provided direct information on the isothermal process of liquid−solid transition. Figure 8 shows

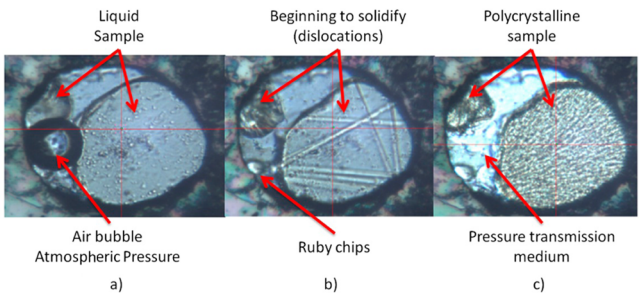

Figure 8. Photomicrographs of Emim[$FeCl_4$] in the sample chamber of MDAC at room temperature under high pressures: (a) 0, (b) 0.35, and (c) 1.05 GPa.

photomicrographs of Emim[$FeCl_4$] with increasing pressure at room temperature, which was visually observed by optical microscopy. It could be seen that the liquid phase of the sample disappeared and solidification gradually occurred. In Figure 8a, we can observe the liquid and an air bubble, indicating that the pressure within the chamber was approximately atmospheric pressure. As the pressure increases, solidification began to take place. At 0.39 GPa (Figure 8b), we can see some lines that correspond to dislocations (beginning to crystallize). When the pressure reached 0.9 GPa (Figure 8c), the crystallization is completed and the polycrystalline nature of the sample could be observed. This result is in good agreement with the solidification of the Emim[BF_4], which is detected at 1.2 GPa.[43]

If we compare these three photomicrographs, we can see that the sample changed gradually from a translucent liquid into a transparent solid phase. This isothermal study is important in order to understand the pressure-induced crystallizing process in ionic liquid Emim[$FeCl_4$], which is associated with the magnetic hysteresis detected around room temperature. Indeed, different weak pressures can control the orientation of iron ions upon solidification, using a constant magnetic field in an isothermal process. These characteristic magnetic features may lead to novel molecular electronic applications using room-temperature magnetic ionic liquids.

CONCLUSIONS

The 1-ethyl-3-methylimidazolium tetrachloroferrate, Emim-[$FeCl_4$], clearly exhibits a long-range antiferromagnetic ordering below the Néel temperature $T_N \approx 3.8$ K. The three-dimensional ordering is strongly influenced by hydrostatic pressure, showing a pressure-induced transition from antiferromagnetic to ferrimagnetic behavior. In addition, this room-temperature ionic liquid is characterized to exhibit a magnetic hysteresis coupled with the liquid−solid phase transition based on alignment of the tetrachloroferrate anion. In particular, it is advantageous that this phenomenon accompanied by hysteresis is originated by weak pressures and magnetic fields near room temperature. These experimental results are interesting in view of new technological applications of MILs, such as chemical switches, molecular sensors, or new devices for separation processes.

ASSOCIATED CONTENT

Supporting Information

Crystal structure below 280 K of Emim[$FeCl_4$]; low-temperature ZFC−FC magnetic susceptibility at two different magnetic fields, 0.01 and 0.1 T, for the pressures of 0.56 and 0.77 GPa; and Raman spectrum of Emim[$FeCl_4$] without applied pressure. This material is available free of charge via the Internet at http://pubs.acs.org.

AUTHOR INFORMATION

Corresponding Author

*E-mail: manuel.depedro@unican.es. Phone: +34 942 201512.

Notes

The authors declare no competing financial interest.

ACKNOWLEDGMENTS

This work was financially supported by MEC research projects MAT2011-27573-C04 and MALTA Consolider Ingenio 2010 program (ref CSD2007-00045).

REFERENCES

(1) Hallett, J. P.; Welton, T. Room-Temperature Ionic Liquids: Solvents for Synthesis and Catalysis. 2. *Chem. Rev.* **2011**, *111*, 3508−3576.

(2) (a) Castner, E. W., Jr.; Wishart, J. F. Spotlight in Ionic Liquids. *J. Chem. Phys.* **2010**, *132*, 120901−120909. (b) Plechkova, N. V.; Seddon, K. R. Applications of Ionic Liquids in the Chemical Industry. *Chem. Soc. Rev.* **2008**, *37*, 123−150.

(3) (a) Giernoth, R. Task-Specific Ionic Liquids. *Angew. Chem., Int. Ed.* **2010**, *49*, 2834−2939. (b) Torimoto, T.; Tsuda, T.; Okazaki, K.; Kuwabata, S. New Frontiers in Materials Science Opened by Ionic Liquids. *Adv. Mater.* **2010**, *22*, 1196−1221. (c) Weingärtner, H. Understanding Ionic Liquids at the Molecular Level: Facts, Problems, and Controversies. *Angew. Chem., Int. Ed.* **2008**, *47*, 654−670.

(d) Mora-Pale, M.; Meli, L.; Doherty, T. V.; Linhardt, R. J.; Dordick, J. S. Room Temperature Ionic Liquids as Emerging Solvents for the Pretreatment of Lignocellulosic Biomass. *Biotechnol. Bioeng.* **2011**, *108*, 1229−1245.
(4) Lane, G. H.; Bayley, P. M.; Clare, B. R.; Best, A. S.; MacFarlane, D. R.; Forsyth, M.; Hollenkamp, A. F. Ionic Liquid Electrolyte for Lithium Metal Batteries: Physical, Electrochemical, and Interfacial Studies of *N*-Methyl-*N*-butylmorpholinium Bis(fluorosulfonyl)imide. *J. Phys. Chem. C* **2010**, *114*, 21775−21785.
(5) (a) Rana, U. A.; Forsyth, M.; MacFarlane, D. R.; Pringle, J. M. Toward Protic Ionic Liquid and Organic Ionic Plastic Crystal Electrolytes for Fuel Cells. *Electrochim. Acta* **2012**, *49*, 213−222. (b) Armand, M.; Endres, F.; MacFarlane, D. R.; Ohno, H.; Scrosati, B. Ionic-liquid Materials for the Electrochemical Challenges of the Future. *Nat. Mater.* **2009**, *8*, 621−629.
(6) Santos, C. E. A.; Alencar, M. A.R.C.; Migowski, P.; Dupont, J.; Hickmanna, J. M. Anionic and Cationic Influence on the Nonlocal Nonlinear Optical Response of Ionic Liquids. *Chem. Phys.* **2012**, *403*, 33−36.
(7) Li, B.; Noda, Y.; Hu, L.; Yoshikawa, H.; Matsushita, M. M.; Awaga, K. Highly Efficient Organic Optoelectronic Conversion Induced by Electric Double Layers in Ionic Liquids. *Appl. Phys. Lett.* **2012**, *100*, 163304.
(8) Bica, K.; Gärtner, P.; Gritsch, P. J.; Ressmann, A. K.; Schröder, C.; Zirbs, R. Micellar Catalysis in Aqueous−Ionic Liquid systems. *Chem. Commun.* **2012**, *48*, 5013−5015.
(9) Tanabe, K.; Suzui, Y.; Hasegawa, M.; Kato, T. Full-Color Tunable Photoluminescent Ionic Liquid Crystals Based on Tripodal Pyridinium, Pyrimidinium, and Quinolinium Salts. *J. Am. Chem. Soc.* **2012**, *134*, 5652−5661.
(10) Branco, A.; Branco, L. C.; Pina, F. Electrochromic and Magnetic Ionic Liquids. *Chem. Commun.* **2011**, *47*, 2300−2302.
(11) Hayashi, S.; Saha, S.; Hamaguchi, H. A New Class of Magnetic Fluids: bmim[$FeCl_4$] and nbmim[$FeCl_4$] Ionic Liquids. *IEEE Trans. Magn.* **2006**, *42*, 12−14.
(12) Monteiro, B.; Gago, S.; Neves, P.; Valente, A. A.; Gonçalves, I. S.; Pereira, C. C. L.; Silva, C. M.; Pillinger, M. Effect of an Ionic Liquid on the Catalytic Performance of Thiocyanatodioxomolybdenum(vi) Complexes for the Oxidation of Cyclooctene and Benzyl Alcohol. *Catal. Lett.* **2009**, *129*, 350−357.
(13) Del Sesto, R. E.; McCleskey, T. M.; Burrell, A. K.; Baker, G. A.; Thompson, J. D.; Scott, B. L.; Wilkes, J. S.; Williams, P. Structure and Magnetic Behavior of Transition Metal Based Ionic Liquids. *Chem. Commun.* **2008**, 447−449.
(14) De Vreese, P.; Brooks, N. R.; Van Hecke, K.; Van Meervelt, L.; Matthijs, E.; Binnemans, K.; Van Deun, R. Speciation of Copper(II) Complexes in an Ionic Liquid Based on Choline Chloride and in Choline Chloride/Water Mixtures. *Inorg. Chem.* **2012**, *51*, 4972−4981.
(15) Nockemann, P.; Thijs, B.; Postelmans, N.; Van Hecke, K.; Van Meervelt, L.; Binnemans, K. Anionic Rare-Earth Thiocyanate Complexes as Building Blocks for Low-Melting Metal-Containing Ionic Liquids. *J. Am. Chem. Soc.* **2006**, *128*, 13658−13659.
(16) Mehdi, H.; Binnemans, K.; Van Hecke, K.; Van Meervelt, L.; Nockemann, P. Hydrophobic Ionic Liquids with Strongly Coordinating Anions. *Chem. Commun.* **2010**, *46*, 234−236.
(17) Mallick, B.; Balke, B.; Felser, C.; Mudring, A. V. Dysprosium Room-Temperature Ionic Liquids with Strong Luminescence and Response to Magnetic Fields. *Angew. Chem., Int. Ed.* **2008**, *47*, 7635−7638.
(18) Tanaka, K.; Ishiguro, F.; Chujo, Y. POSS Ionic Liquid. *J. Am. Chem. Soc.* **2010**, *132*, 17649−17651.
(19) Miao, C.; Wang, J.; Yu, B.; Cheng, W.; Sun, J.; Chanfreau, S.; He, L.; Zhang, S. Synthesis of Bimagnetic Ionic Liquid and Application for Selective Aerobic Oxidation of Aromatic Alcohols under Mild Conditions. *Chem. Commun.* **2011**, *47*, 2697−2699.
(20) Eliseeva, S. V.; Bünzli, J. C. G. Lanthanide Luminescence for Functional Materials and Bio-sciences. *Chem. Soc. Rev.* **2010**, *39*, 189−227.
(21) (a) Okuno, M.; Hamaguchi, H.; Hayashi, S. Magnetic Manipulation of Materials in a Magnetic Ionic Liquid. *Appl. Phys. Lett.* **2006**, *89*, 132506. (b) Raeissi, S.; Peters, C. J. *Green Chem.* **2009**, *11*, 185−192.
(22) Jiang, Y.; Guo, C.; Liu, H. Magnetically Rotational Reactor for Absorbing Benzene Emissions by Ionic Liquids. *China Particuol.* **2007**, *5*, 130−133.
(23) Olivier-Bourbigou, H.; Magna, L.; Morvan, D. Ionic Liquids and Catalysis: Recent Progress from Knowledge to Applications. *Appl. Catal., A* **2010**, *373*, 1−56.
(24) Ko, N. H.; Lee, J. S.; Huh, E. S.; Lee, H.; Jung, K. D.; Kim, H. S.; Cheong, M. Extractive Desulfurization Using Fe-Containing Ionic Liquids. *Energy Fuels* **2008**, *22*, 1687−1690.
(25) Albo, J.; Santos, E.; Neves, L. A.; Simeonov, S. P.; Afonso, C. A. M.; Crespo, J. G.; Irabien, A. Separation Performance of CO_2 through Supported Magnetic Ionic Liquid Membranes (SMILMs). *Sep. Purif. Technol* **2012**, *97*, 26−33.
(26) Funasako, Y.; Mochida, T.; Inagaki, T.; Sakurai, T.; Ohta, H.; Furukawad, K.; Nakamura, T. Magnetic Memory Based on Magnetic Alignment of a Paramagnetic Ionic Liquid Near Room Temperature. *Chem. Commun.* **2011**, *47*, 4475−4477.
(27) Mikkola, J. P.; Virtanen, P.; Sjöholm, R. Aliquat 336® - A Versatile and Affordable Cation Source for an Entirely New Family of Hydrophobic Ionic Liquids. *Green Chem.* **2006**, *8*, 250−255.
(28) (a) Yoshida, Y.; Otsuka, A.; Saito, G.; Natsume, S.; Nishibori, E.; Takata, M.; Sakata, M.; Takahashi, M.; Yoko, T. Conducting and Magnetic Properties of 1-Ethyl-3-methylimidazolium (EMI) Salts Containing Paramagnetic Irons: Liquids [EMI][M'III'Cl4] (M = Fe and Fe0.5Ga0.5) and Solid $[EMI]_2$[Fe'II'Cl4]. *Bull. Chem. Soc. Jpn.* **2005**, *78*, 1921−1928. (b) Yoshida, Y.; Saito, G. Influence of Structural Variations in 1-Alkyl-3-methylimidazolium Cation and Tetrahalogenoferrate(III) Anion on the Physical Properties of the Paramagnetic Ionic Liquids. *J. Mater. Chem.* **2006**, *16*, 1254−1262.
(29) (a) de Pedro, I.; Rojas, D. P.; Albo, J.; Luis, P.; Irabien, A.; Blanco, J. A.; Rodríguez Fernández, J. Long-Range Magnetic Ordering in Magnetic Ionic Liquid: Emim[FeCl4]. *J. Phys.: Condens. Matter.* **2010**, *22*, 296006. (b) de Pedro, I.; Rojas, D. P.; Blanco, J. A.; Rodríguez Fernández, J. Antiferromagnetic Ordering in Magnetic Ionic Liquid Emim[$FeCl_4$]. *J. Magn. Magn. Mater.* **2011**, *323*, 1254−1257.
(30) Bäcker, T.; Breunig, O.; Valldor, M.; Merz, K.; Vasylyeva, V.; Mudring, A. In-Situ Crystal Growth and Properties of the Magnetic Ionic Liquid [C_2mim][$FeCl_4$]. *Cryst. Growth Des.* **2011**, *11*, 2564−2571.
(31) (a) Yoshimura, Y.; Takekiyo, T, H. Pressure-Induced Spectral Changes of Room-Temperature Ionic Liquid, *N*,*N*-Diethyl-*N*-methyl-*N*-(2-methoxyethyl)ammonium Bis(trifluoromethylsulfonyl)imide, [DEME][TFSI]. *J. Phys. Chem. C* **2012**, *116*, 2097−2101. (b) Takekiyo, T.; Imai, Y.; Hatano, N.; Abe, H.; Yoshimura, Y. Conformational Preferences of Two Imidazolium-Based Ionic Liquids at High Pressures. *Chem. Phys. Lett.* **2011**, *511*, 241−246.
(32) Smith, T. F.; Chu, C. W.; Maple, M. B. Superconducting Manometers for High Pressure Measurement at Low Temperature. *Cryogenics* **1969**, *9*, 53−56.
(33) Syassen, K. Ruby under Pressure. *High Press. Res.* **2008**, *28*, 75−126.
(34) Néel, L. Proprietés Magnétiques des Ferrites: Ferrimagnétisme et Antiferromagnétismo. *Ann. Phys. (Paris, Fr.)* **1948**, *3*, 137−198.
(35) Alfonso, B. F.; Piqué, C.; Trobajo, C.; García, J. R.; Kampert, E.; Zeitler, U.; Rodríguez Fernández, J.; Fernández-Díaz, M. T.; Blanco, J. A. Neutron Powder Diffraction Investigation in Ammonium Iron(III) Bis(hydrogenphosphate). *Phys. Rev. B* **2010**, *82*, 144431.
(36) (a) Talaty, E. R.; Raja, S.; Storhaug, V. J.; Dölle, A.; Carper, W. R. Raman and Infrared Spectra and ab Initio Calculations of C_{2-4}MIM Imidazolium Hexafluorophosphate Ionic Liquids. *J. Phys. Chem. B* **2004**, *108*, 13177. (b) Sitze, M. S.; Schreiter, E. R.; Patterson, E. V.; Freeman, R. G. Ionic Liquids Based on $FeCl_3$ and $FeCl_2$. Raman Scattering and ab Initio Calculations. *Inorg. Chem.* **2001**, *40*, 2298−2304.

(37) Kim, J. Y.; Kim, J. T.; Song, E.; Min, Y.; Hamaguchi, H. Polypyrrole Nanostructures Self-Assembled in Magnetic Ionic Liquid as a Template. *Macromolecules* **2008**, *41*, 2886−2889.
(38) Heimer, N. E.; Del Sesto, R. E.; Meng, Z.; Wilkes, J. S.; Carper, W. R. Vibrational Spectra of Imidazolium Tetrafluoroborate Ionic Liquids. *J. Mol. Liq.* **2006**, *124*, 84−95.
(39) Umebayashi, Y.; Fujimori, T.; Sukizaki, T.; Asada, M.; Fujii, K.; Kanzaki, R.; Ishiguro, S. Evidence of Conformational Equilibrium of 1-Ethyl-3-methylimidazolium in Its Ionic Liquid Salts: Raman Spectroscopic Study and Quantum Chemical Calculations. *J. Phys. Chem. A* **2005**, *109*, 8976−8982.
(40) Ozawa, R.; Hayashi, S.; Saha, S.; Kobayashi, A.; Hamaguchi, H. Rotational Isomerism and Structure of the 1-butyl-3-methylimidazolium Cation in the Ionic Liquid State. *Chem. Lett.* **2003**, *32*, 948−949.
(41) Fumino, K.; Wulf, A.; Ludwig, R. Strong, Localized, and Directional Hydrogen Bonds Fluidize Ionic Liquids. *Angew. Chem., Int. Ed.* **2008**, *47*, 8731−8734.
(42) Luzón, J.; Campo, J.; Palacio, F.; McIntyre, G. J.; Millán, A. The Role of the Hydrogen Bond in the Magnetic Interaction Mechanisms of $A_2FeX_5{\cdot}H_2O$ (A = Rb, K, X = Cl, Br): A Polarized Neutron Diffraction Study and ab Initio Calculations. *Phys. Rev. B.* **2008**, *78*, 054414.
(43) Takekiyo, T.; Hatano, N.; Abe, H.; Yoshimura, Y. High Pressure Raman Study on the Local Structure of 1-Ethyl-3-methylimidazolium Tetrafluoroborate. *High Press. Res.* **2012**, *32*, 150−154.